Optimal control of crystallization of alpha-lactose monohydrate

Amira Rachah, Dominikus Noll, Fabienne Espitalier, Fabien Baillon

Optimal control of crystallization of alpha-lactose monohydrate*

A. Rachah† D. Noll† F. Espitalier‡ F. Baillon†

Abstract

We present a mathematical model for solvated crystallization of α-lactose monohydrate in semi-batch mode. The process dynamics are governed by conservation laws including population, molar and energy balance equations. We present and discuss the model and then control the process with the goal to privilege the production of small particles in the range between 10^{-5} and $10^{-4}\mu m$. We compare several specific and unspecific cost functions leading to optimal strategies with significantly different effects on product quality. Control inputs are temperature, feed rate, and the choice of an appropriate crystal seed.

1 Introduction

Crystallization is the unitary operation of formation of solid crystals from a solution. In process engineering crystallization is an important separation process used in chemical, pharmaceutical, food, material and semiconductor industries. Mathematical models are described by conservation laws with population, molar and energy balance equations. Crystallizers can be operated either in batch, semi-batch or continuous mode. Semi-batch crystallization is widely used in the pharmaceutical and fine chemical industry for the production of solids in a variety of operating modes.

Crystallization processes are described by balance equations, including a population balance for the particle size distribution, a molar balance for the distribution of solute, and an energy balance equation to model thermodynamic phenomena. In the food-processing industry, there has

*Draft of accepted article in IEEE *Asian Control Conference (ASCC 2013)*.

†Université Paul Sabatier, Institut de Mathématiques, Toulouse, France

‡Ecole des Mines d'Albi, Centre Rapsodee, Albi, France

been a growing interest in the crystallization of lactose in recent years [4, 5, 7]. In this paper we study a model of solvated crystallization of α-lactose monohydrate, which includes four interacting populations, one of them aging, in tandem with an energy balance. Two forms of lactose (α- and β-lactose) exist simultaneously in aqueous solution, the exchange being governed by mutarotation.

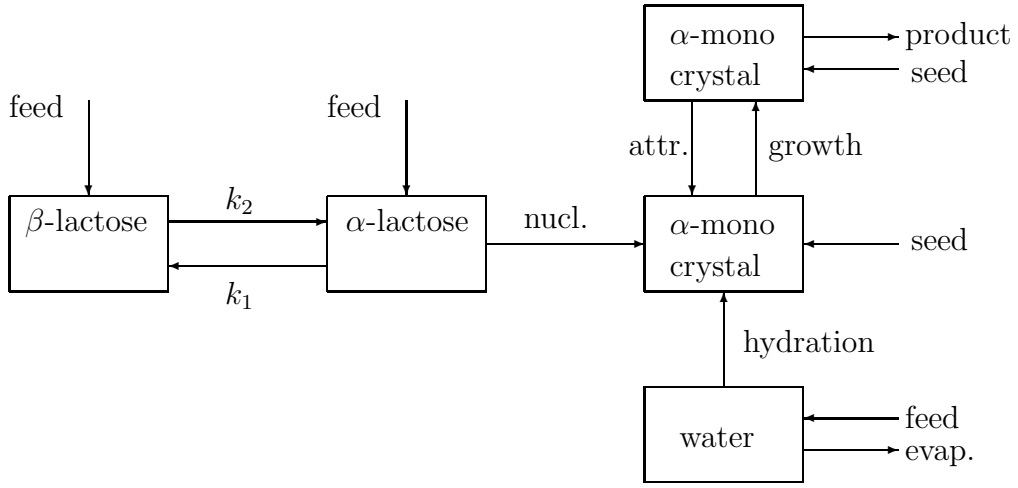

FIGURE 1: Solvated crystallization of α-lactose monohydrate with complex population dynamics featuring one aging and three ageless populations. Exchange rates depend on temperature. Controls are feed rate in semi-batch mode, temperature of envelope, and the distribution of the crystal seed. Based on mathematical modeling the process is optimized in order to maximize the particle mass in a given small size range $L_{\text{low}} \leq L \leq L_{\text{high}}$.

Crystallization and precipitation processes are modeled as highly nonlinear and complex dynamical systems. This makes it interesting to simulate, control and optimize these processes in order to enhance product quality in various situations [1, 2]. In order to control crystallization processes, Hu and Rohani [3] have studied different heuristic cooling methods such as linear cooling, natural cooling and controlled cooling. In this study we control of the process of formation of α-lactose crystals in such a way that the growth of very large crystals is avoided and the bulk of crystal mass occurs in a small particle range between 10^{-5} and $10^{-4}\mu m$. In order to achieve this goal we use optimal control of the process in semi-batch mode by variations of temperature, feed rate, and also by an appropriate choice of the crystal seed, and based on a variety of different figure of merit functions.

2 Dynamic model of process

In this section the dynamic model of semi-batch crystallization of α-lactose monohydrate is described by presenting the population, molar and energy balance equations.

Population balance equation: The population balance equation is a first-order PDE

$$\frac{\partial}{\partial t}\left(V(t)n(L,t)\right) + V(t)G\left(c_\alpha(t), c_\beta(t), T(t)\right)\frac{\partial n(L,t)}{\partial L} = V(t)\dot{n}(L,t)^{\pm}, \tag{1}$$

where $n(L,t)$ is the distribution of α-lactose crystals, $c_\alpha(t), c_\beta(t)$ are the dimensionless concentrations of α- and β-lactose in the liquid phase, $V(t)$ is the volume of slurry in the crystallizer, a dependent variable given in (11), $G\left(c_\alpha, c_\beta, T\right)$ is the temperature-dependent growth coefficient of α-crystals, assumed independent of crystal size L, and the right hand side represents source and sink terms. We add the boundary condition

$$n(0,t) = \frac{B\left(c_\alpha(t), c_\beta(t), T(t)\right)}{G\left(c_\alpha(t), c_\beta(t), T(t)\right)}, \tag{2}$$

and the initial condition

$$n(L,0) = n_0(L), \tag{3}$$

where $n_0(L)$ is the crystal seed. It is convenient to introduce the moments of the crystal size distribution function

$$\mu_\nu(t) = \int_0^\infty n(L,t)L^\nu dL, \quad \nu = 0, 1, \ldots,$$

which allows to break (1) into an infinite sequence of ODEs if the source and sink terms may be neglected. In the present situation this amounts to neglecting agglomeration and also attrition effects. Using (2) we obtain the equations

$$\frac{d\mu_\nu(t)}{dt} + \frac{V'(t)}{V(t)}\mu_\nu(t) - \nu G\left(c_\alpha(t), c_\beta(t), T(t)\right)\mu_{\nu-1}(t) = 0, \tag{4}$$

$\nu = 1, 2, \ldots$, in tandem with

$$\frac{d\mu_0(t)}{dt} + \frac{V'(t)}{V(t)}\mu_0(t) - B\left(c_\alpha(t), c_\beta(t), T(t)\right) = 0. \tag{5}$$

The initial conditions are then

$$\mu_\nu(0) = \int_0^\infty n_0(L)L^\nu dL, \quad \nu = 0, 1, \ldots.$$

Solvent mass balance:

$$\frac{dm_{\mathrm{H_2O}}(t)}{dt} = (R^{-1} - 1)3k_v\rho_{\mathrm{cry}}G\left(c_\alpha(t), c_\beta(t), T(t)\right)V(t)\mu_2(t) + q_{\mathrm{H_2O}}(t) \tag{6}$$

Here $m_{\mathrm{H_2O}}$ is the mass of water in the aqueous solution, which changes due to feed, $q_{\mathrm{H_2O}}$, and due to the integration of water molecules into the α-crystals. The constant $R = M_{\mathrm{cry}}/M_\alpha = 1.0525$ is the ratio of the molar masses of the solid and liquid phases of α-lactose.

Concentration of α-lactose: The dimensionless concentration of α-lactose c_α in the solution is defined as $m_\alpha = c_\alpha m_{\mathrm{H_2O}}$ and satisfies the differential equation

$$\begin{aligned}\frac{dc_\alpha(t)}{dt} = \quad & \frac{1}{m_{\mathrm{H_2O}}(t)}[c_\alpha(t)(1-R^{-1}) - R^{-1}]\frac{dm_{\mathrm{cry}}(t)}{dt} - k_1(T(t))c_\alpha(t) + k_2(T(t))c_\beta(t) \\ & + (c_\alpha^+(t) - c_\alpha(t))\,\frac{q_{\mathrm{H_2O}}(t)}{m_{\mathrm{H_2O}}(t)}.\end{aligned} \tag{7}$$

Here m_{cry} is the crystal mass in the slurry, c_α^+ is the feed rate of α lactose during the semi-batch phase, and $k_1(T)$, $k_2(T)$ are the temperature dependent mutarotation exchange rates between α- and β-lactose in the liquid phase.

Concentration of β-lactose: The dimensionless concentration of β-lactose c_β is defined as $m_\beta = c_\beta m_{\mathrm{H_2O}}$ and satisfies the differential equation

$$\begin{aligned}\frac{dc_\beta(t)}{dt} \quad & = \frac{c_\beta(t)}{m_{\mathrm{H_2O}}(t)}(1-R^{-1})\frac{dm_{\mathrm{cry}}(t)}{dt} + k_1(T(t))c_\alpha(t) - k_2(T(t))c_\beta(t) \\ & + \left(c_\beta^+(t) - c_\beta(t)\right)\frac{q_{\mathrm{H_2O}}(t)}{m_{\mathrm{H_2O}}(t)}.\end{aligned} \tag{8}$$

Energy balance: The temperature hold system describes the interaction between crystallizer temperature, the temperature of the jacket, and the control signal, to which the internal heat balance due to enthalpy is added. We have

$$\begin{aligned}\frac{dT(t)}{dt} = P_1(t)\Bigg[& - P_2(t)(T(t) - T_{\mathrm{ref}}) - \Delta H\frac{dm_{\mathrm{cry}}(t)}{dt} + UA(t)\left(T_{\mathrm{jacket}}(t) - T(t)\right) \\ & + q_{\mathrm{H_2O}}(t)\left(C^p_{\mathrm{H_2O}} + C^p_\alpha c_\alpha(0) + C^p_\beta c_\beta(0)\right)\left(T_{\mathrm{feed}} - T_{\mathrm{ref}}\right)\Bigg]\end{aligned} \tag{9}$$

where

$$\frac{dT_{\mathrm{jacket}}(t)}{dt} = -0.0019(T_{\mathrm{jacket}}(t) - T_{\mathrm{sp}}(t)) \tag{10}$$

was obtained through identification of the system. Here $T(t)$ is the temperature of the slurry, $T_{\mathrm{ref}} = 25^0$C a constant reference temperature, T_{feed} the temperature of feed, which is the temperature of H_2O in this case, assumed constant in this study, $T_{\mathrm{jacket}}(t)$ is the temperature of the crystallizer jacket, and $T_{\mathrm{sp}}(t)$ is the set point temperature, which is used as a control input to regulate $T_{\mathrm{jacket}}(t)$, and therefore indirectly $T(t)$ via the heat exchange between the envelope and the crystallizer through the contact surface $A(t)$, which is determined through $V(t)$. The constants $C^p_{\mathrm{H_2O}}$, C^p_α, C^p_β are the specific heat capacities. We have

$$P_1(t)^{-1} = m_{\mathrm{H_2O}}(t)C^p_{\mathrm{H_2O}} + m_\alpha(t)C^p_\alpha + m_\beta(t)C^p_\beta + m_{\mathrm{cry}}(t)C^p_{\mathrm{cry}},$$

$$P_2(t) = \frac{dm_{\mathrm{H_2O}}(t)}{dt}C^p_{\mathrm{H_2O}} + \frac{dm_\alpha(t)}{dt}C^p_\alpha + \frac{dm_\beta(t)}{dt}C^p_\beta + \frac{dm_{\mathrm{cry}}(t)}{dt}C^p_{\mathrm{H_2O}},$$

with $m_\alpha = c_\alpha m_{\mathrm{H_2O}}$, $m_\beta = c_\beta m_{\mathrm{H_2O}}$.

Mutarotation: The mutarotation exchange coefficients k_1, k_2 are temperature dependent and are determined as

$$k_2(T) = k_0 \cdot \exp(-E/(R \cdot (T + 273.15))),$$

$$k_m(T) = 1.64 - 0.0027 \cdot T, k_1(T) = k_2(T) \cdot k_m(T).$$

The equilibrium of mutarotation therefore occurs at

$$c_{\alpha,\mathrm{sat,eq}}(T) = \frac{10.9109 \cdot \exp(0.02804 \cdot T)}{100(1 + k_m(T))},$$

$$F(T) = 0.0187 \cdot \exp(0.0236 \cdot T),$$

$$c_{\alpha,\mathrm{sat}}(c_\beta, T) = c_{\alpha,\mathrm{sat,eq}}(T) - F(T)(c_\beta - k_m(T) \times c_{\alpha,\mathrm{sat,eq}}(T)).$$

Nucleation rate: The nucleation rate is based on a phenomenological law

$$B(c_\alpha, c_\beta, T) = k_b \exp\left(-\frac{B_0}{(T + 273.15)^3 \ln^2\left(\frac{c_\alpha}{c_{\alpha,\mathrm{sat}}(c_\beta,T)}\right)}\right)$$

as is the growth rate

Growth rate:

$$G(c_\alpha, c_\beta, T) = k_g \left(c_\alpha - c_{\alpha,\mathrm{sat}}(c_\beta, T)\right).$$

Volume: The total volume of slurry $V(t)$ is a dependent variable, which can be expressed as a function of the states c_α, c_β and $m_{\mathrm{H_2O}}$ through

$$V(t) = \frac{m_{\mathrm{H_2O}}(t)}{1 - k_v \mu_3(t)} \left[\rho_{\mathrm{lac},\alpha}^{-1} c_\alpha(t) + \rho_{\mathrm{lac},\beta}^{-1} c_\beta(t) + \rho_{\mathrm{H_2O}}^{-1}\right]. \tag{11}$$

Therefore

$$\frac{dV(t)}{dt} = 3k_v G(c_\alpha(t), c_\beta(t), T(t)) V(t) \mu_2(t) + \frac{dm_{\mathrm{H_2O}}(t)}{dt} \left[\rho_{\mathrm{lac},\alpha}^{-1} c_\alpha(t) + \rho_{\mathrm{lac},\beta}^{-1} c_\beta(t) + \rho_{\mathrm{H_2O}}^{-1}\right] + m_{\mathrm{H_2O}}(t) \left(\rho_{\mathrm{lac},\alpha}^{-1} \frac{dc_\alpha(t)}{dt} + \rho_{\mathrm{lac},\beta}^{-1} \frac{dc_\beta(t)}{dt}\right).$$

Crystal mass: The total crystal mass satisfies the equation

$$\frac{dm_{\mathrm{cry}}(t)}{dt} = 3k_v \rho_{\mathrm{cry}} G(c_\alpha(t), c_\beta(t), T(t)) V(t) \mu_2(t). \tag{12}$$

R	1.0525	–	ratio of molar masses
k_v	0.523598	–	volumic shape factor
ρ_{cry}	1545	$kg \cdot m^{-3}$	crystal density
$\rho_{\text{lac},\alpha}$	1545	$kg \cdot m^{-3}$	α-lactose density
$\rho_{\text{lac},\beta}$	1590	$kg \cdot m^{-3}$	β-lactose density
$\rho_{\text{H}_2\text{O}}$	1000	$kg \cdot m^{-3}$	water density
ΔH	-43.1	kJ/kg	heat of crystallization
U	300	$kJ/m^2.h.K$	heat transfert coefficient
k_0	$2.25 \cdot 10^8$	s^{-1}	kinetic mutarotation constant
T_{ref}	25	^0C	reference temperature
$C^p_{\text{H}_2\text{O}}$	4180.5	$J/kg/K$	heat capacity H_2O
C^p_{cry}	1251	$J/kg/K$	heat capacity α-lactose monohydrate
C^p_α	1193	$J/kg/K$	heat capacity α-lactose
C^p_β	1193	$J/kg/K$	heat capacity β-lactose
B_0	5.83		nucleation constant
R_g	18.314	$J/K/mol$	universal gas constant
k_g	$10 \cdot 10^{10}$	$m \cdot s^{-1}$	growth rate coefficient
k_b	$1.18 \cdot 10^{-7}$	$\sharp \cdot m^{-3} s^{-1}$	birth rate coefficient
t_f	11000	s	final time for study 1
c^+_α	0.521	kg/kg water	fraction of α-lactose in feed
c^+_β	0.359	kg/kg water	fraction of β-lactose in feed
V_0	0.0015	m^3	initial volume
$V_{\max}$	0.01	m^3	maximum volume

TABLE 1: Numerical constants

3 Optimal control problem

The benefit of the moment approach is that we may choose a finite number of moment equation to replace (1). Our present approach is to retain a sufficient number of moments so that the salient features of the seed $n_0(L)$ may be captured by these moments, and in our experiments we decided

$n(L,t)$	$\sharp/m.m^3$	particle size distribution
$m_\alpha(t)$	kg	mass of α-lactose in solution
$m_\beta(t)$	kg	mass of β-lactose in solution
$V(t)$	kg	volume of slurry
$A(t)$	m^2	contact surface

TABLE 2: Units of dynamic quantities

to retain the moments $\mu_0, \ldots, \mu_5$. The remaining states of the system dynamics are then $m_{\mathrm{H_2O}}$, m_{cry}, c_α, c_β, T, T_{jacket}. The control inputs are $u_1 = T_{\mathrm{sp}}$ and $u_2 = q_{\mathrm{H_2O}}$.

μ_0	1.24051^{10}	$m_{\mathrm{H_2O}}$	0.92kg
μ_1	2.176710^6	c_α	0.359
μ_2	409.2491	c_β	0.521
μ_3	0.0812	T	70^0C
μ_4	1.681210^{-5}	T_{jacket}	20^0C
μ_5	3.609410^{-9}		

TABLE 3: Initial values for study 1

In this work, we compare between several policies :

- Policy 1 : We fix the values of the set-point temperature $T_{\mathrm{sp}} = 15[^0C]$ and the feed rate of solvent $q_{\mathrm{H_2O}} = 0.0056[Kg/h]$. This policy is referred to as *constant* in the figures.
- Policy 2 : Here we fix the value of the feed rate of solvent $q_{\mathrm{H_2O}} = 0.0056[Kg/h]$, while the set-point temperature $T_{\mathrm{sp}}(t)$ starts at $T_{\mathrm{sp}}(0) = 15[^0C]$ and decreases linearly. This policy is called *linear* in the figures.
- Policy 3 : We control the set-point temperature $u_1(t) = T_{\mathrm{sp}}(t)$ and also the feed rate of solvent $u_2(t) = q_{\mathrm{H_2O}}(t)$ using various objectives. This policy is called *optimal* in the figures.

3.1 Scenario 1

Our first control problem minimizes the weighted mean size diameter $d_{43} = \dfrac{\mu_4}{\mu_3}$ at fixed final time $t_f = 11000$ seconds. This is cast as the optimization program

$$\begin{aligned} \text{minimize} \quad & d_{43}(t_f) = \frac{\mu_4(t_f)}{\mu_3(t_f)} \\ \text{subject to} \quad & \text{dynamics } (4) - (12) \\ & 0 \leq V(t) \leq V_{\max} \\ & 0^0\text{C} \leq T(t) \leq 70^0\text{C} \\ & c_\alpha(t) \geq c_{\alpha,\text{sat}}(c_\beta(t), T(t)) \\ & 0^0\text{C} \leq T_{\text{sp}}(t) \leq 40^0\text{C} \\ & 0 \leq q_{\text{H}_2\text{O}}(t) \leq 0.1 \end{aligned} \tag{13}$$

The control variables are set-point temperature $u_1(t) = T_{\text{sp}}(t)$ and feed rate of water $u_2(t) = q_{\text{H}_2\text{O}}(t)$. The percentages $\dot{c}_\alpha^+$ and $\dot{c}_\beta^+$ of lactose in the feed are kept constant.

3.2 Scenario 2

Our second control problem minimizes the nucleation rate $B(c_\alpha, c_\beta, T)$ at the fixed final time $t_f = 11000$ seconds. This is cast as the optimization program

$$\begin{aligned} \text{minimize} \quad & B(t_f) \\ \text{subject to} \quad & \text{constraints of } (13) \end{aligned} \tag{14}$$

The control variables are again T_{sp} and $q_{\text{H}_2\text{O}}$.

3.3 Scenario 3

Our third control problem minimizes the coefficient of variation CV at the fixed final time $t_f = 11000$ seconds. This is the optimization program

$$\begin{aligned} \text{minimize} \quad & CV(t_f) = \frac{\mu_3(t_f)\mu_5(t_f)}{(\mu_4(t_f))^2} - 1 \\ \text{subject to} \quad & \text{constraints of } (13) \end{aligned} \tag{15}$$

The control variables are again T_{sp} and $q_{\text{H}_2\text{O}}$.

In Figures 2, 3 we present results obtained with the optimal regulation of set-point temperature $u_1 = T_{\text{sp}}$ and feed rate $u_2 = q_{\text{H}_2\text{O}}$ and compare these to more standard scenarios, where temperature and feed rate are fixed or follow simple heuristic profiles proposed in the literature.

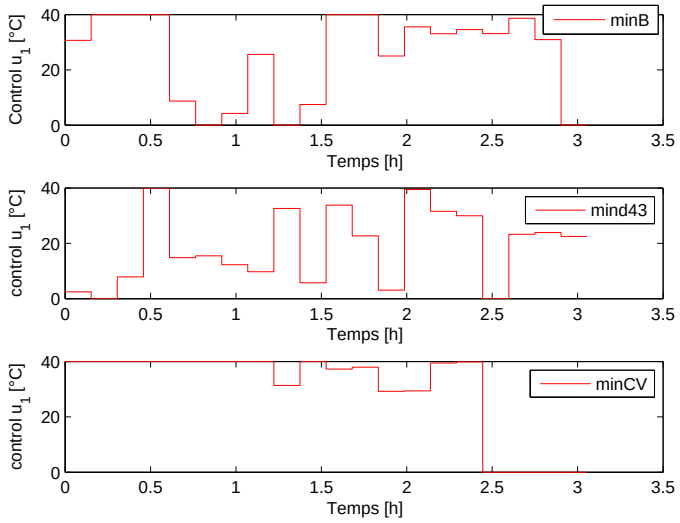

FIGURE 2: Optimal set-point temperature profile $u_1 = T_{\text{sp}}$ for minimization of the three criteria B, CV and d_{43} with fixed final time t_f.

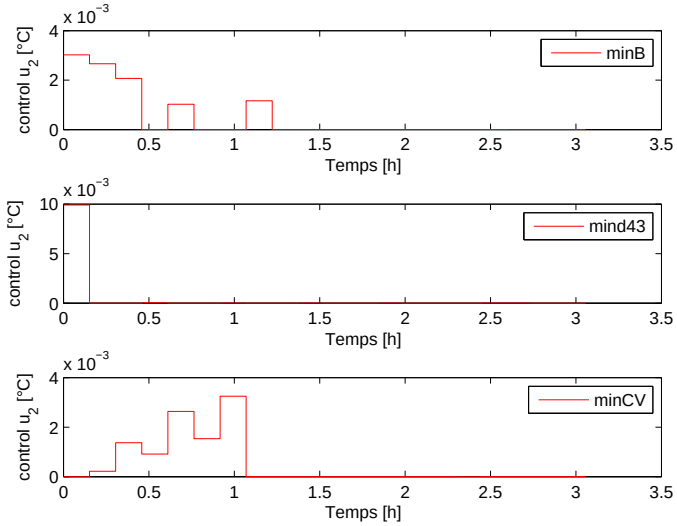

FIGURE 3: Optimal feed profile $u_2 = q_{\text{H}_2\text{O}}$ for minimization of the three criteria B, d_{43} and CV with fixed final time t_f.

In Figure 4 we present the optimal crystal size distribution obtained from minimization of the weighted mean size diameter d_{43} in (13) compared with standard scenarios. Figure 5 shows the crystal size distribution for the optimal control of nucleation rate B and coefficient of variation CV compared to the more standard scenarios. The optimal profile for the nucleation rate shows the existence of two peaks which indicates the existence of two populations of crystals.

In Figure 6 we present the evolution of solubility of $\alpha-$lactose and the temperature of the crystallizer by comparing several scenarios. The profile of solubility shows an early peak, which

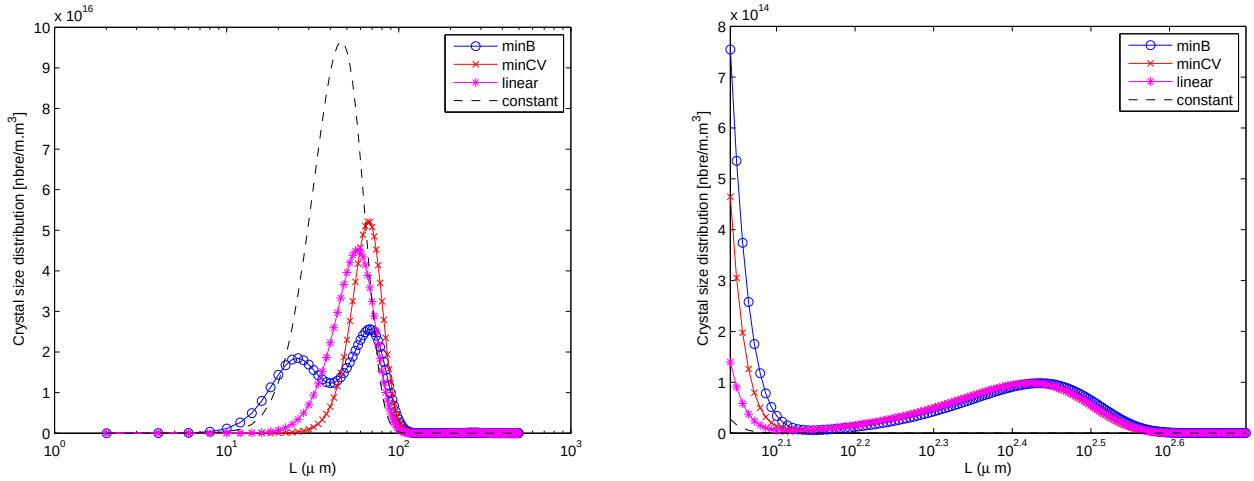

FIGURE 4: Final crystal size distribution $L \mapsto n(L, t_f)$ displayed for minimization of B (blue) and CV (red) compared with linear (magenta) and constant (dashed black) policies for fixed final time t_{final}. Right hand image shows zoom on range $[10^{2.1}, 10^{2.6}]$.

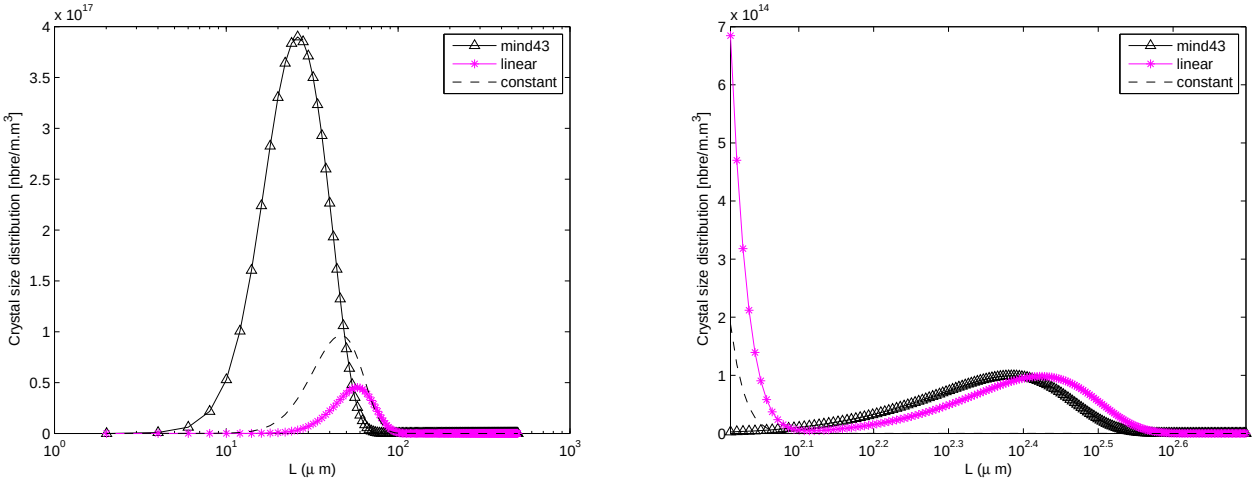

FIGURE 5: Final crystal size distribution $L \mapsto n(L, t_f)$ for minimizing d_{43} (black solid), compared with linear (magenta) and constant (black dashed) policies for fixed final time t_{final}. Right hand image shows zoom on range $[10^{2.1}, 10^{2.6}]$.

correspond to a sharp decrease in the temperature profile of the crystallizer. Comparison between the cost functions shows that the highest peak occurs when minimizing the weighted mean size diameter d_{43}. In the case of minimization of nucleation rate B, we see the existence of two peaks which correspond with two peaks on crystal size distribution profile.

In Figure 7 we present the evolution of nucleation rate B and growth rate G in comparison between the several scenarios. At the beginning of the profile of nucleation rate B, we note the highest peak in case of minimization of weighted mean size diameter d_{43}.

In Figure 8 we present the coefficient of variation CV and volume of crystallizer in comparison

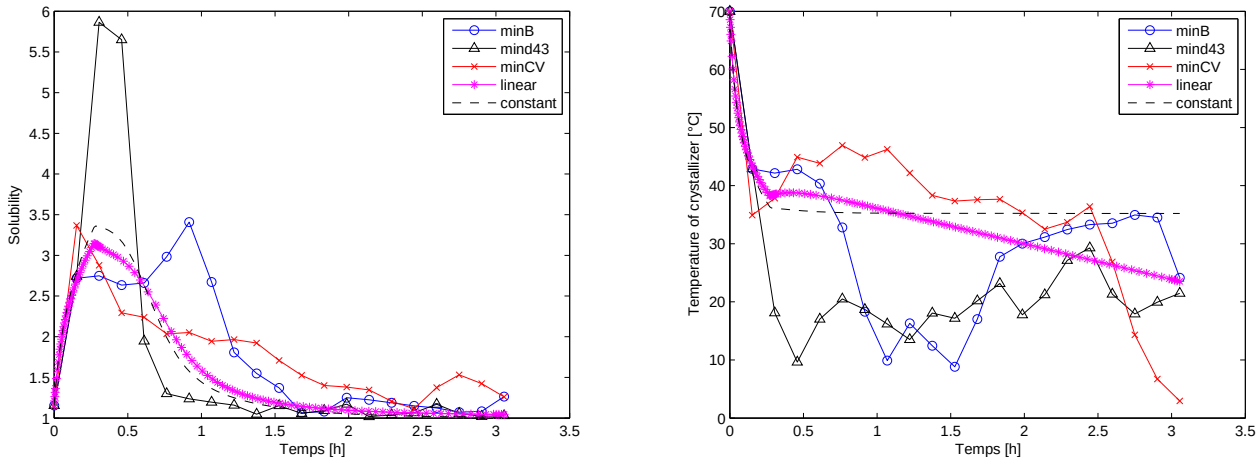

FIGURE 6: Left image compares solubility, right image compares temperature of crystallizer for the five policies constant (dashed black), linear (magenta), optimal with B (blue), optimal with CV (red) and optimal with d_{43} (black continuous) for t_{final} fixed.

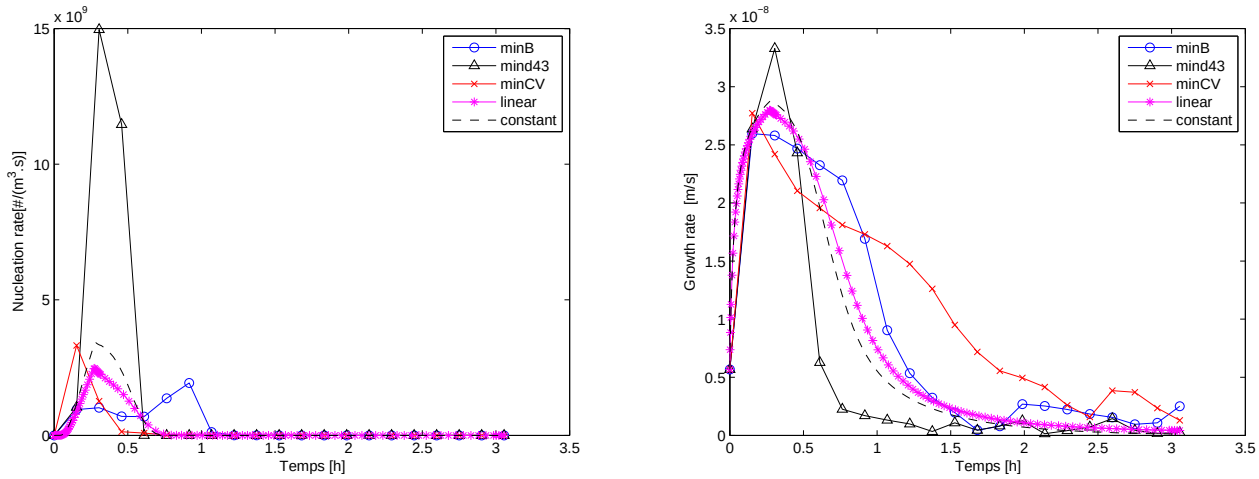

FIGURE 7: Left image compares growth rate, right image compares crystal mass for the five policies constant (dashed black), linear (magenta), optimal with B (blue), optimal with CV (red), optimal with d_{43} (black continuous) for t_{final} fixed.

between all objectives and scenarios. The volume profiles show that optimization of different cost functions may lead to fairly different ways of filling the crystallizer in the semi-batch phase. For instance, filling in the linear policy occurs much faster than for minimization of the coefficient of variation, which gives the slowest filling.

Figure 9 compares the profiles of overall crystals mass and of the weighted mean size diameter d_{43} in all scenarios.

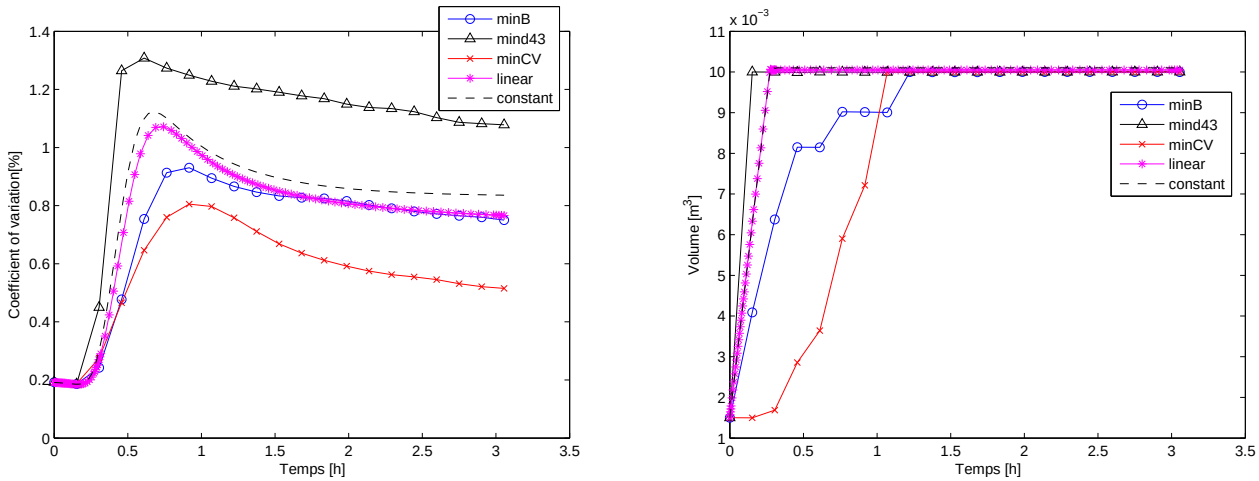

FIGURE 8: Evolution of coefficient of variation $CV(t)$ left, evolution of volume $V(t)$ right. Comparison of the five policies constant (dashed black), linear (magenta), optimal for B (blue), optimal for CV (red), optimal for d_{43} (black continuous), for t_{final} fixed.

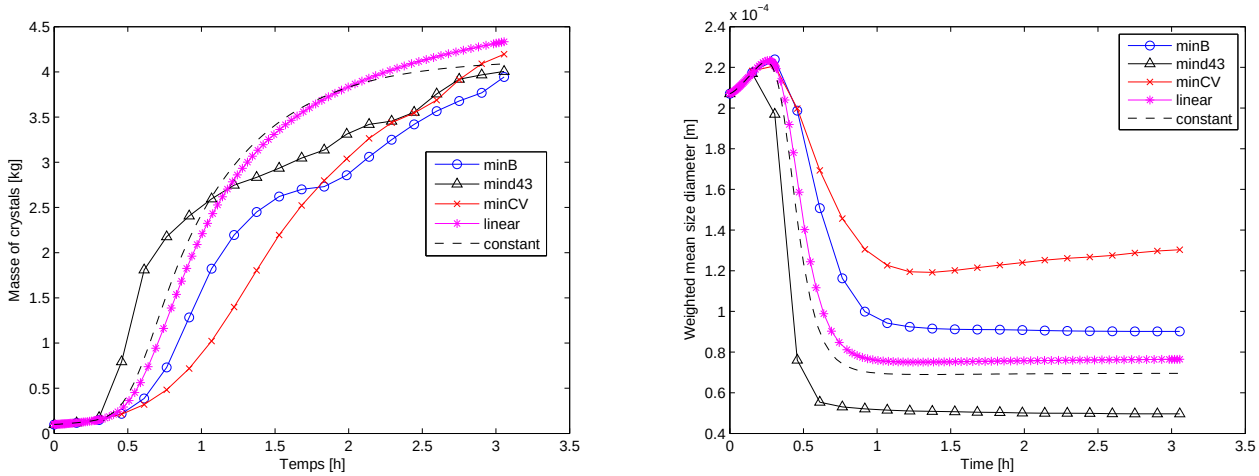

FIGURE 9: Evolution of weighted mean size diameter d_{43} left, evolution of crystal mass right. Comparison of the five policies constant (dashed black), linear (magenta), optimal for B (blue), optimal for CV (red), optimal for d_{43} (black continuous), for t_{final} fixed.

3.4 Scenario 4

The next extension is to add the moments of $n_0(L)$ as unknown parameters, the idea being that a suitable choice of the initial seed of given mass should give even better results. We decide to fix the total mass of crystal seed as $k_v V_0 \rho_{\text{cry}} \int_0^\infty n_0(L) L^3 dL = 0.1\text{kg}$. That leads to the optimization

program

$$\begin{array}{ll} \text{minimize} & d_{43} \\ \text{subject to} & \text{constraints of (14)} \\ & \mu_3(0) = \int_0^\infty n_0(L) L^3 dL = 0.0812 \end{array} \tag{16}$$

where now $T_{\text{ref}}(t)$, $q_{\text{H}_2\text{O}}(t)$ and $\mu_0(0)$, $\mu_1(0)$, $\mu_2(0)$, $\mu_4(0)$, $\mu_5(0)$ are optimization variables.

The interesting point of this program is that once the optimal solution $(T^*_{\text{ref}}, q^*_{\text{H}_2\text{O}}, \mu^*_\nu)$ is reached, we need to reconstruct a function $n^*_0(L)$ such that its moments $0, \ldots, 5$ coincide with $\mu^*_0, \mu^*_1, \mu^*_2, \mu^*_3 = 0.0812, \mu^*_4, \mu^*_5$. This can be achieved by solving the maximum entropy function reconstruction problem

$$\begin{array}{ll} \text{minimize} & \int_0^\infty n_0(L) \log n_0(L) dL \\ \text{subject to} & \int_0^\infty L^\nu n_0(L) dL = \mu^*_\nu, \nu = 0, \ldots, 5. \end{array} \tag{17}$$

Notice that (17) may be solved by standard software, see e.g. Borwein *et al.* [8], [9].

3.5 Scenario 5

The natural figure of merit to maximize the crystal mass within a certain range $L_1 \leq L \leq L_2$ of small particle sizes is

$$\max \int_{L_1}^{L_2} L^3 n(L, t_f) dL \tag{18}$$

at the final time t_f, but this objective is not directly accessible in the moment approach. Substrates like B, CV, d_{43} are non-specific and must be expected to give only a crude approximation of (18). We therefore propose the following more sophisticated strategy, which is compatible with the moment approach.

We define a target particle size distribution $n_1(L)$, which has a bulk in the range $[L_1, L_2]$, normalized to satisfy

$$\nu_3 = \int_0^\infty L^3 n_1(L) dL = 1.$$

Then we compute as many of its moments $\nu_0, \ldots, \nu_N$ as we wish to use, where as before $N = 5$ in our tests. The optimization program we now solve is

$$\begin{array}{ll} \text{minimize} & \sum_{i=0}^{N} w_i \left(\mu_i(t_f) - \mu_3(t_f)\nu_i\right)^2 \\ \text{subject to} & \text{constraints of (13)} \\ & t_f \leq t_{\max} \end{array} \tag{19}$$

where the w_i are suitably chosen weights. Notice that the least squares objective of (19) tries to bring the moments of $n(L, t_f)$ as close as possible to the moments of the function $\mu_3(t_f)n_1(L)$, which has the correct shape, and has the same total crystal mass as $n(L, t_f)$. Here the final time is considered free.

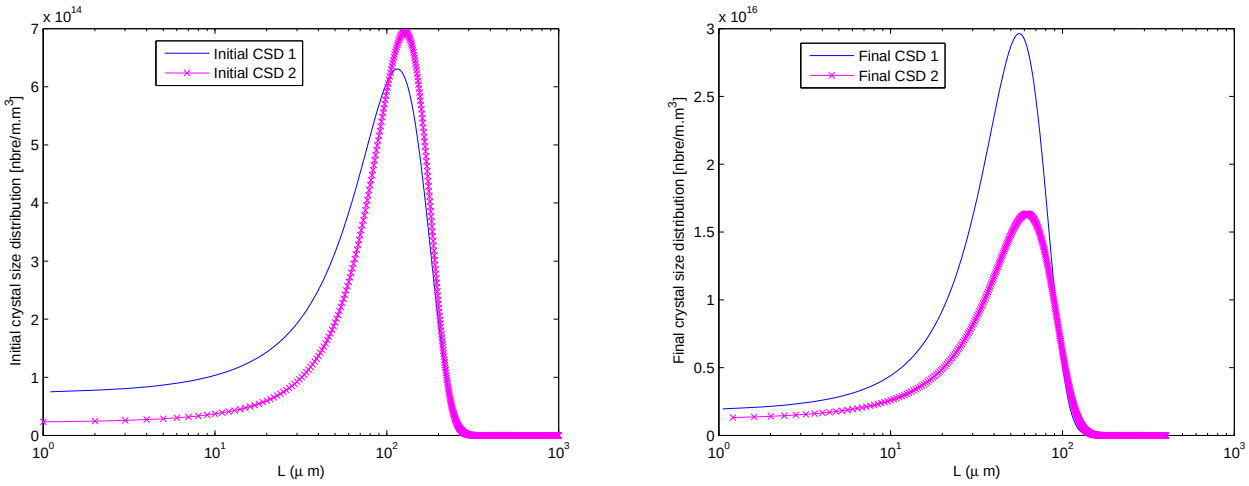

FIGURE 10: Scenario 5: Different initial seeds $n_0(L)$ shown on the left lead to different products $n(L, t_f)$ on the right. Blue uses $\mu_3(0) = 0.291$, magenta uses $\mu_3(0) = 0.401$.

4 Method

For our testing we have used the solver ACADO [10] based on a semi-direct single or multiple-shooting strategy, including automatic differentiation, based ultimately on the semi-direct multiple-shooting algorithm of Bock and Pitt [11]. ACADO is a self-contained public domain software environment written in `C++` for automatic control and dynamic optimization.

Alternatively, we also use the solver PSOPT [12], which is a public domain extension of the NLP-slover IPOPT [13] or SNOPT [14] and is based on pseudospectral optimization which uses Legendre or Cheybyshev polynomials and discretization based on Gauss-Lobatto nodes.

A difficulty with both solvers is the strong dependence of convergence and solutions on the initial guess, as must be expected in a local optimization context. Our testing shows that it is often mandatory to have a simulated study $(x_{\text{init}}, u_{\text{init}})$ available to start the optimization from that point. This initial guess may use parameters from a previous optimization study, which give already a decent cost in the present study. In some cases homotopy techniques, using for instance t_f as a parameter, have to be used.

Once optimal controls $u^* = (T^*_{\text{ref}}, q^*_{\text{H}_2\text{O}})$ have been computed in any one of the scenarios, we use the full crystallizer model (1), (2), (6) – (10) to simulate the system, using an initial seed $n_0(L)$

which produces the initial moments $\mu_\nu(0)$. In those cases where the moments of the initial seed are parameters, which are also optimized, we use the optimal $\mu^* = (\mu_0^*, \ldots, \mu_N^*)$ to compute an estimation $n_0^*(L)$ of the optimal crystal seed with these moments using [8] and [9].

The final stage in each experiment is a simulation of the full population balance model using the optimal $(T_{\text{sp}}^*, q_{\text{H}_2\text{O}}^*, n_0(L)^*)$, obtained from the moment-based optimal control problem.

5 Conclusion

We have presented and tested several control strategies which allow to maximize the crystal mass of particles of small size, typically in a range of $10^{-5} - 10^{-4}\mu m$. Our approach was compared to more standard heuristic control policies used in the literature to regulate temperature and feed rate in semi-batch mode. Our simulated numerical results show that it is beneficial to apply optimal control strategies in semi-batch solvated crystallization of α-lactose monohydrate.

References

[1] A. Randolph, M. A. Larson (1988). Theorie of particulate processes, Academic Press Inc, San Diego, CA, Second Edition.

[2] James B. Rawling, Walter R. Witkowski and John W.Eaton (1992). Modelling and control of crystallizers, Powder technology, volume 6.

[3] Q. Hu, S.Rohani, D.X. Wang, A. Jutan (2005). Optimal control of a batch cooling seeded crystallizer, Powder technology, volume 7.

[4] J. Mcleod (2007). Nucleation and growth of Alpha lactose Monohydrate PhD Thesis, Massey University, volume 220.

[5] A. Mimouni (2007). Cristallisation du Lactose et épaississement dans les Lactosérums concentrés, PhD Thesis, Ecole Nationale Supérieure Agronomique de Rennes.

[6] Y. Shi, B. Liang, R.W. Hartel (1990). Isothermal crystallization of alpha-lactose monohydrate in a continuous cooling crystallizer, Journal of Food Science, volume 55.

[7] A. Mimouni, P. Schuck, S. Bouhallab (2009). Isothermal batch crystallisation of alpha-lactose: A kinetic model combining mutarotation, nucleation and growth steps, International Dairy Journal, volume 8.

[8] J.B. Borwein, A. S. Lewis On the convergence of moment problems, American Mathematical Society, Volume 23, Number 1 , May 1991.

[9] J.B. Borwein, A. S. Lewis, M .N. Limber, D. Noll Maximum entropy reconstruction using derivative information part 2: computational results, Numerische Mathematik, Volume 14,May 1995.

[10] D. Ariens, B. Houska, H.J. Ferreau (2010). ACADO Toolkit User's Manual. `http://www.acadotoolkit.org.`

[11] H.G. Bock, K.J. Pitt (1984). A multiple shooting algorithm for direct solution of optimal control problems. Proc 9th IFAC World Congress, Budapest, pp. 243 – 247. Pergamon Press.

[12] http://www.psopt.org/Home

[13] A. Wachter and L. T. Biegler. On the Implementation of a Primal-Dual Interior Point Filter Line Search Algorithm for Large-Scale Nonlinear Programming. Mathematical Programming, 2006. `https://projects.coin-or.org/Ipopt`.

[14] P. E. Gill, Walter Murray, and M. A. Saunders. SNOPT: An SQP algorithm for Large-Scale Constrained Optimization. SIAM Review, 47(1), 2001. `http://www.sbsi-sol-optimize.com/asp/sol product snopt.htm`.